Chapter 9

Power Generation with Thermolytic Reverse Electrodialysis for Low-Grade Waste Heat Recovery

Deok Han Kim, Byung Ho Park, Kilsung Kwon, Longnan Li and Daejoong Kim

Additional information is available at the end of the chapter

http://dx.doi.org/10.5772/intechopen.81006

Abstract

Closed-loop reverse electrodialysis (RED) systems that use a thermolytic solution for low-grade waste heat recovery have attracted significant attention. They have several cost benefits, e.g., the absence of repetitive pretreatment and removal of locational constraints, when compared with open-loop RED systems using seawater and river water. This study presents a model of RED that uses ammonium bicarbonate, and this is a promising solution for closed-loop systems. The modified Planck-Henderson equation is used to calculate the ion exchange membrane potential. The calculation is based on the conductivity measurements as ionization carbonate electrochemical information has not been reported before this study. The solution resistance is experimentally determined. The experimentally obtained permselectivity is implemented into the model to predict the membrane potential more accurately. The results of the improved model are well matched with experimental results under results under various operating conditions of the RED system. In addition, in the model of this study, the net power density was characterized with the consideration of the pumping loss. The improved model predicts a maximum net power density of 0.84 W/m^2 with an intermembrane distance of 0.1 mm, a flow rate of 3 mL/min, and a concentration ratio of 200 as optimum conditions. The results of the study are expected to improve our understanding of the ammonium bicarbonate-RED system and contribute to modeling studies using ammonium bicarbonate or certain other compounds for novel technologies of waste heat recovery.

Keywords: reverse electrodialysis (RED), closed-loop, waste heat, ammonium bicarbonate, thermolytic solution

1. Introduction

The increase in world energy consumption has led to a significant increase in the demand for fossil fuels. The increase in fossil fuel consumption causes various problems, including global warming and climate change. The Paris climate conference underscores the collective, world-wide attention on preventing bigger disasters. Several studies have focused on lessening and replacing the consumption of fossil fuels. An emerging source is waste heat, which is not only a cause of heat pollution but also a source for generating electricity in a different way [1, 2]. There are several techniques to harness waste heat, e.g., the organic Rankine cycle (ORC) and thermoelectric power. However, there are several disadvantages for the recovery of energy by using these techniques, such as environmentally harmful refrigerants, downsizing in ORC systems, low efficiency, and poor form factor in thermoelectric elements [3–9].

The reverse electrodialysis (RED) system combined with thermal separation components could form a closed loop that harnesses the waste heat by utilizing the salinity gradient energy (SGE) [10]. RED is a power generation technique based on SGE. RED mixes of two different salinity solutions with ion exchange membranes (IEM). It includes advantage of not emitting environmentally harmful gases. It also obtains unlimited, free fuel supply in the vicinity of places where seawater and river water meet. Conversely, the accessibility to these natural resources limits its locational options. Furthermore, the high cost of maintenance of the RD stack is a challenging problem for actual implementation. Especially, the IEMs, a core component, are still exposed to fouling problems, and the fouled IEMs should be either replaced with new ones or recovered [11, 12]. These problems of RED can be overcome by combining a RED system with a thermal separation component because of its closed-loop characteristics [13–16]. The difference of salinity solution concentrations retains the electromotive force by separating the increased solute from the diluted side and recapturing it in the concentrated solution without any fresh solution supply, and thus the process is operated as a closed-loop system. The closed-loop system mitigates the geographical limitations as a continuous supply of fresh seawater (high concentration solution) and river water (low concentration solution) is not necessary, thereby preventing the possible risks of membrane fouling as well as saving pretreatment costs.

A thermolytic solution that is easily separated at a relatively low temperature is necessary for the process. Traditionally, organic and ammonia solutions are used as thermolytic solutions in waste heat recovery systems. Organic solutions, such as R-21 and R-123, have a low boiling point; however, they do not solve in water and show low osmotic efficiency [4]. Ammonia water (ammonium hydroxide) is another widely used ORC solution; however, it is corrosive, which means the damage of the materials of RED such as membranes and spacers. An ammonium bicarbonate is a promising thermolytic solution owing to its high solubility in water, large osmotic efficiency, circulation capacity, and relatively low molecular weight [17, 18]. More importantly, ammonium bicarbonate can be recovered with moderate heat, which suggests significant energy advantages compared with the regeneration of other draw solutes. Ammonium bicarbonate has low decomposition temperature, of approximately 60°C at 1 atm, and it decomposes at 120°C. Luo et al. conducted RED experiments by using an ammonium bicarbonate solution under different inlet conditions. They set different feed

solution flow rate and feed solution concentration combinations [10]. They achieved a maximum power density of 0.89 W/m^2 with an intermembrane distance of 0.3 mm and with concentrated and diluted solutions of 2 and 0.02 M, respectively [19]. Kwon and his coworkers quantitatively tested parameters such as intermembrane distances and IEM types [20]. They obtained a power density of 0.77 W/m^2 with an intermembrane distance of 0.2 mm and with concentrated and diluted solutions of 1.5 and 0.01 M, respectively. Geise et al. provided deep insights into the transport phenomena of ammonium bicarbonate through IEMs [21–24]. They analyzed the relationship between the permselectivity, membrane resistance, membrane structure, and functional groups fixed on several types of IEMs and individual ion species of the ammonium bicarbonate electrolyte.

Since 2011, the studies have focused on RED numerical simulations. Veerman et al. developed a one-dimensional numerical model for a unit cell [25]. Tedesco et al. improved the model of Veerman with respect to the previously neglected nonideal phenomena, such as concentration polarization (CP) and temperature variation, and validated a wider concentration range [26]. Kwon and his coworkers further developed the model. They applied some updated thermodynamic properties in the model, such as dielectric constant and viscosity. CP phenomena were considered in their model through the implementation with empirical equations. This upgraded model can predict the actual physics more accurately, and it enabled the calculation of higher concentration combinations. However, the calculation with bicarbonate is yet to be improved because of its complexity. Compared to a binary electrolyte (e.g., sodium chloride), it is hard to of extensively expressing the electrochemical information.

The key issue in this calculation is to predict the internal resistance and membrane potential in the system. Compared with NaCl, which is the conventional electrolyte for the RED process, the electrochemical information of ammonium bicarbonate requires the estimation of the membrane potential and internal resistance, including activity and transport number. The transportation properties of ammonium bicarbonate remain unclarified and unexplored by extant studies. A recent study estimated the membrane potential based on electrical conductivity measurements [27]. The solution resistance was computed in the range of concentration of our interest based on the definition of molar conductivity.

In this study, we performed a numerical simulation of RED power generation. The simulation was based on ammonium bicarbonate and validated through our experimental results. The permselectivity of the IEM was assumed as in previous studies [25, 26, 28]. Moreover, we measured all the properties by an experiment to predict the RED performance more precisely. Following the model validation, the optimum operating conditions of RED systems were characterized with different settings in terms of flow rate, intermembrane distance, and concentration ratio.

2. Modeling approach

A thermal-driven electrochemical generator (TDEG) is illustrated in **Figure 1**. The TDEG consists of a RED system and a separator based on thermal energy [10]. The mixed diluted

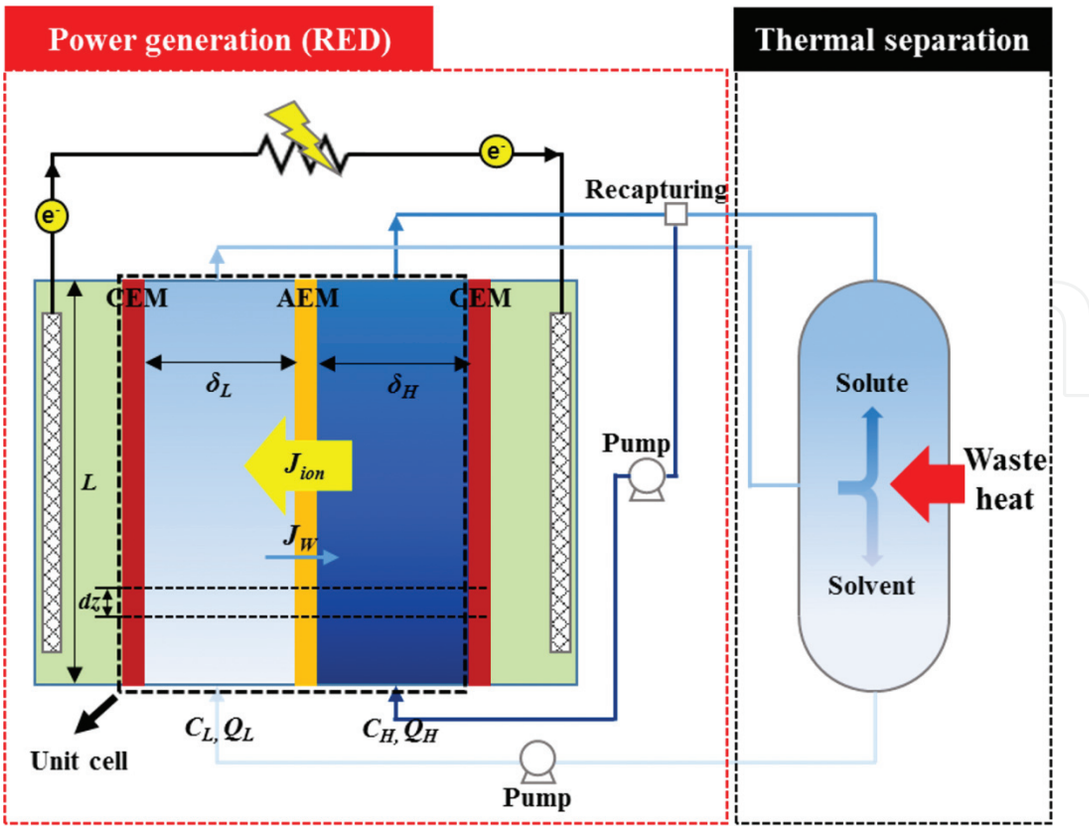

Figure 1. Schematic illustration of a TDEG. The figure on the left-hand side shows an RED single-cell model, and it has a flow length of *L*. The solution flows through the channel (thickness δ) with a flow rate of Q.

solution can be separated by applying waste heat in the separator. Then, it will be recaptured in the concentrated solution. Specifically, electricity would be generated when the high concentration and low concentration ammonium bicarbonate solutions flow through each side of the IEM. Meanwhile, ions would pass though the membrane, and the two solutions with different concentrations are mixed. Then, the flow stream would flow into a thermal separator (e.g., a distillation column). Waste heat is utilized in the thermal separator to separate the solute (NH_3 and CO_2) from the concentration flow stream. The solute from the thermal separator would be recaptured by the high concentration flow stream to form a renewed high concentration flow stream, which is supplied to the RED again. Thus, the renewed high and low concentration streams flow back to the RED stack. The concentration gradient between the different sides of the IEM is maintained. A unit cell pair in RED is composed of a concentrated solution channel, a diluted solution channel, a cation exchange membrane (CEM), and an anion exchange membrane (AEM). The solution concentrations are estimated along the channel with length *L* and width *W* in this study.

The present model was developed based on the following four assumptions [25]: (1) the resistance of the IEMs is held at a constant value; (2) the electrode potential of a stack is linearly proportional to the number of cells; (3) the effect of the electrodes at both ends of the stack is neglected; and (4) the inlet flow is uniformly distributed into each channel.

The input parameters used in the model are listed in **Table 1**.

When we consider the RED system as an electric circuit, the RED stack exhibits potential difference and internal resistance. Equation (1) shows the potential difference across an IEM between two solutions of different concentration, which is described for all ionic species present in the solution [31]:

$$V(z) = \frac{R_g T}{F} \sum_i \frac{t_i}{z_i} \ln\left(\frac{\gamma_i^H C_i^H(z)}{\gamma_i^L C_i^L(z)}\right) \quad (1)$$

Here, T denotes the temperature, R_g denotes the universal gas constant (8.314 J/mol·K), F denotes the Faraday constant (96485 C/mol), C denotes the concentration of solution, z_i denotes the valence number of ion species i, and γ denotes the activity coefficient.

The definition of ionic transport number for species i (t_i) is the ionic flux of that species divided by the overall ionic current across the IEM membrane. The electrochemical information of ammonium bicarbonate is needed when calculating equating membrane potential. This is because the equilibrium and ionization constant of ammonium bicarbonate were not clear [27]. Given that Eq. (1) is not intuitive to determine transport number and activity of

Spacer properties		
Open ratio (—)		0.56
Porosity (—)		0.74
Solution properties		
Diffusivity of ammonium bicarbonate (m^2/s) [a]		1×10^{-12}
Diffusivity of water (m^2/s)		1.2×10^{-9}[29]
IEMs' properties		
CEM	Resistance ($\Omega \cdot cm^2$) [b]	2 [23]
	Permselectivity (—)	Experiment
	Thickness (m)	120 [29]
AEM	Resistance ($\Omega \cdot cm^2$) [b]	12 [23]
	Permselectivity (—)	Experiment
	Thickness (m)	120 [29]

[a]From extant studies [26], the stack performance is not significantly affected by the diffusivity of NaCl for a wide range (two order magnitude). We verified the same tendency on an ammonium bicarbonate electrolyte for a wider range (three order magnitude), between 1×10^{-11} and 1×10^{-14} m^2/s, because of the heavier molecular weight of ammonium bicarbonate than that of NaCl [30]. Thus, the value of 1×10^{-12} m^2/s is considered as a reliable assumption.
[b]The membrane resistance was measured through the direct current (DC) method at 0.5 M ammonium bicarbonate on both sides [23].

Table 1. Input parameters used in the RED model.

ammonium bicarbonate compared with NaCl [25, 26, 30, 32], Huang et al. adopted the Planck-Henderson equation to compute the membrane potential as below [27, 31]:

$$V(z) \approx \frac{R_g T}{F} \frac{\sum \frac{|z_i| u_i}{z_i} \left[C_i^L(z) - C_i^H(z) \right]}{\sum |z_i| u_i \left[C_i^L(z) - C_i^H(z) \right]} \ln \left(\frac{\sum |z_i| u_i C_i^H(z)}{\sum |z_i| u_i C_i^L(z)} \right) \tag{2}$$

In this equation, we assume that the activity of each species is proportional to the ionic mobility (u_i) and the molar concentration (C_i). Here, we assume that the valence number of all electrolytes in the ammonium bicarbonate solution is dominantly monovalent (+1 or −1) which can be measured by the pH of the solution [27].

For the binary electrolyte, Eq. (2) is transformed into Eq. (3) by imposing the electrical conductivity described in Eq. (4) and the permselectivity of the IEM [33–39]:

$$V \approx \alpha_{IEM} \frac{R_g T}{F} \ln \left(\frac{\kappa^H}{\kappa^L} \right) \tag{3}$$

$$\kappa = F \sum |z_i| u_i C_i \tag{4}$$

The total internal resistance in the system is computed by the following Eq. (5):

$$R_{ohmic}(z) = \frac{1}{\beta} \left(R_{CEM} + R_{AEM} + \frac{\delta_H}{\Lambda_H(z) C_H(\mathbf{z})} + \frac{\delta_L}{\Lambda_L(z) C_L(\mathbf{z})} \right) \tag{5}$$

Here, δ denotes the thickness of the channels, β denotes an open ratio of the spacer, and Λ denotes the molar conductivity of the solutions. The third and fourth terms in the right-hand side denote the resistance of the solution bodies. R_{CEM} and R_{AEM} denote the resistances of the IEMs measured by the direct current method under standard conditions [23, 39].

The previous Falkenhagen-Leist-Kelbg (FLK) equation describes the molar conductivity generally based on an NaCl solution, and here, we modified it for the case of ammonium bicarbonate [26, 32]. We utilized empirical values by using the definition of electrical conductivity of ammonium bicarbonate ($\Lambda = \kappa / C$) obtained by conductivity measurements as shown in **Figure 2**. The Arrhenius law [40] shows that if a temperature variation exists, then a new electrical conductivity profile must be established such that the electrical conductivity increases with the increase in temperature based on the Arrhenius law [40].

The current value is calculated by Ohm's law, which is based on the system voltage and resistance, as follows:

$$I(z) = \frac{V_{OC}(z)}{R_{\text{int}}(z) + R_{load}} \tag{6}$$

Here, the subscripts *int* and *load* mean the internal resistance of the cell and external resistance, respectively. The current density i is obtained by integrating $I(z)$ along the channel. Then, the

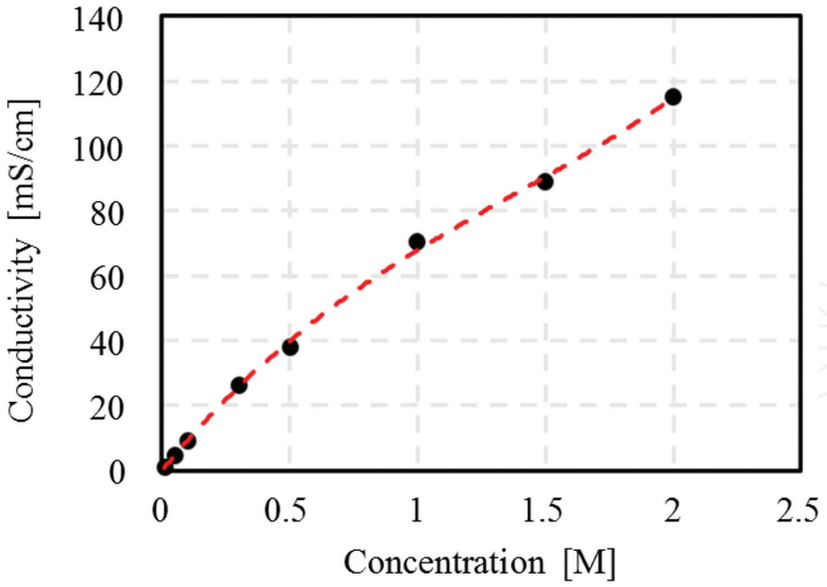

Figure 2. Electrical conductivity of ammonium bicarbonate solution for various concentrations. The red dashed line denotes a third order regression line and $R^2 = 0.99$.

current value is divided by the projecting membrane area. The factor 1/2 is related to the pair membrane area (CEM and AEM) in a cell as follows:

$$i = \frac{\sum_{z=0}^{L} I(z)dz}{2LW} \tag{7}$$

Finally, the power output and power density of the system can be calculated as Eq. (8):

$$\boldsymbol{P}(z) = \boldsymbol{I}(z)^2 \boldsymbol{R}_{load} \tag{8}$$

$$p = \frac{\sum_{z=0}^{L} P(z)dz}{2LW} \tag{9}$$

Equation (10) shows the total solute transportation (flux) in the system. The total solute flux (J_s) can be divided into two different parts. The first term of the right-hand side of the equation indicates the counter-ion transport through the membrane, and it is the coulombic part. The other term in the right-hand side shows the co-ion transport. The co-ion transport can be expressed by the diffusivity (D_{AmBi}) of ammonium bicarbonate and the ion exchange membrane thickness (h) [25]:

$$J_s(z) = \frac{i(z)}{F} + \left(\frac{D_{AmBi}}{h_{CEM}} + \frac{D_{AmBi}}{h_{AEM}} \right) \left(C_H(z) - C_L(z) \right) \tag{10}$$

Another mass transport phenomenon that happens in the system is water flux across the membrane, which is in the opposite direction owing to the osmosis [29] caused by the concentration difference across the IEM;

$$J_w(z) = -\left(\frac{D_w}{h_{CEM}} + \frac{D_w}{h_{AEM}}\right)\left(C_H(z) - C_L(z)\right) \tag{11}$$

Here, D_w denotes the water diffusivity.

The concentration profile along the flow channel is calculated by mass conservation equations for an infinitesimal control volume as follows [25]:

$$\frac{dC_H}{dz}(z) = -\frac{W}{Q_H}J_s(z) + C_H(z)\frac{W}{Q_H}J_w(z)V_w \tag{12}$$

$$\frac{dC_L}{dz}(z) = \frac{W}{Q_L}J_s(z) - C_L(z)\frac{W}{Q_L}J_w(z)V_w \tag{13}$$

Here, V_w denotes the water molar density.

First, the feed solution concentration and solution flow rate are assigned to the model as the input conditions. Second, the local electric variables are calculated. Finally, the next node concentration is obtained through Eqs. (12) and (13) with the solute and water transport. The backward finite difference approximation with a node size of $dz = L/3000$ is applied.

3. Experimental approach

3.1. Experimental setup for RED

In the experiment, instead of NaCl, ammonium bicarbonate (11213, Sigma-Aldrich) was used. **Figure 3(a)** illustrates the RED stack, which includes two electrodes combined with endplates, CEMs and AEMs, silicon gaskets, and polymer spacers. The endplates were fabricated with polymethyl methacrylate (PMMA). The electrodes combined with the endplates were fabricated by titanium and coated with iridium and ruthenium. The calibration of the membranes (CMV/AMV, Asahi glass) was performed in a 0.6 M NH_4HCO solution for more than 24 h after washed by deionized water. The RED stack consists of five cells, and the effective membrane area was 49 cm^2. The polymer spacers (PETEX 06–745/56, Sefar) were used as the channel supporter, and the vertical material exchange is precipitated in the channel to prevent forming the boundary layer. The gaskets were composed of silicone rubber sheets with a thickness of 0.3 mm. The gaskets and spacers were cut in the desired 5 M K_4 $Fe(CN)_6$ (31254, Sigma-Aldrich), 0.05 M $K_3Fe(CN)_6$ (31253, Sigma-Aldrich), 0.05 $K_4Fe(CN)_6$ (31254, Sigma-Aldrich), and 0.3 M NH_4HCO_3. Those experiments were carried out at the room temperature of 25 ± 0.3°C.

Figure 3(b) shows the RED experimental setup. All the solutions were fed by peristaltic pumps (EMP-2000 W, EMS Tech). A four-wire mode cable was connected to the electrodes, and a source meter (2410, Keithley) was employed to measure the RED performance. We used polarization and power density curves to characterize the RED system electrochemical performance. We measured the terminal voltage over the stack by the galvanostat method with the

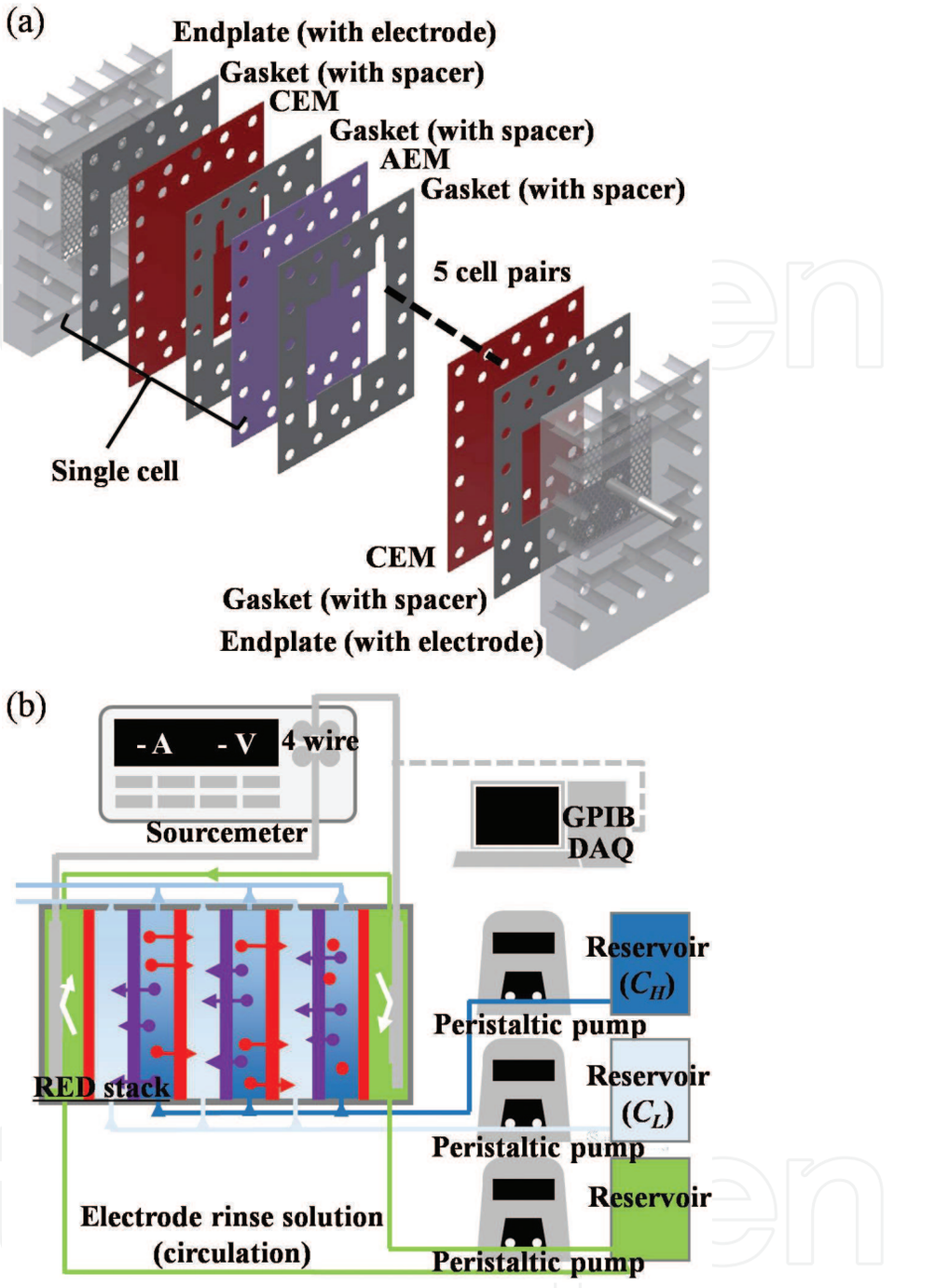

Figure 3. Schematic illustration of (a) the RED stack and (b) the RED experimental setup. The red and purple colors in the schematic indicate the cation and anion, respectively (e.g., cation or cation exchange membrane).

current variation in a step-like way of 10 mA. The power density curve is determined according to the voltage and the current density.

3.2. Membrane potential measurement

In previous studies related to the RED numerical model, permselectivity was assumed as either unity or a constant value. However, it was reported that the permselectivity of an IEM

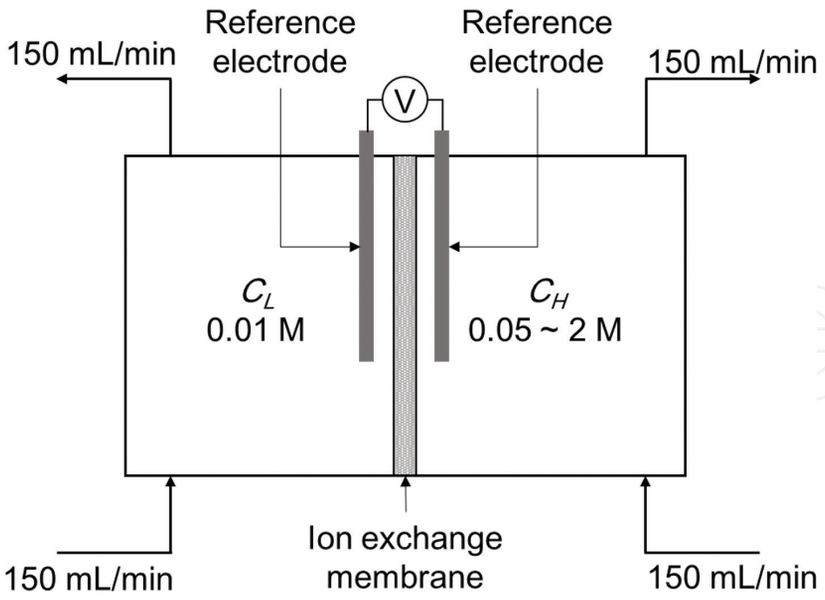

Figure 4. Schematic illustration of the experimental setup to determine the permselectivity of the IEM.

varies with different combinations of the concentrated and diluted solutions [22, 27, 36, 41]. Therefore, to predict the RED performance more precisely, we applied the actual permselectivity of the IEMs as follows.

The permselectivity is calculated by the following equation [39]:

$$\alpha = \frac{\Delta V_{actual}}{\Delta V_{theoretical}} \tag{14}$$

To calculate permselectivity, a simple experiment was needed to measure the IEM potential. **Figure 4** shows the method we used to measure permselectivity. Two reservoirs contain solutions with different concentration combinations. Two reference electrodes and an IEM are inserted between the reservoirs [42, 43]. Ag/AgCl is used as reference electrode, as it has a very low potential. The total area of the IEM was 0.785 cm^2, and the solution contained in each reservoir was 100 mL. In order to reduce the CP effect, the solutions were circulated, and the membrane potential was measured by the Ag/AgCl electrodes after 15–30 min when the system reached a steady state [39].

4. Results and discussion

4.1. Application of actual permselectivity

In **Figure 5**, the conductivity-based estimation of the membrane potential is presented with a blue line, which is calculated by Eq. (4). Here, α is set to unity. The experimental membrane potentials across each IEM are denoted as circular and triangular symbols. For each case, the

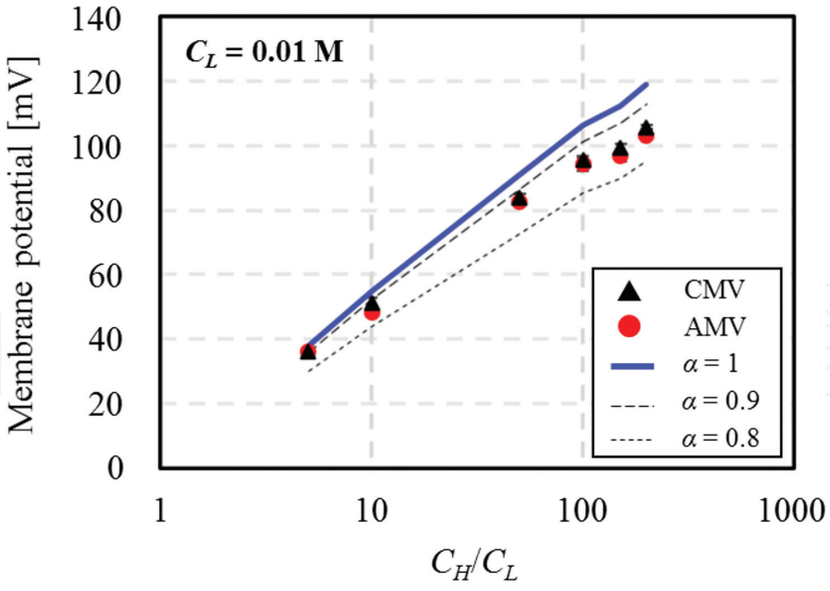

Figure 5. Comparison of the experimental membrane potential data (circular and triangular symbols) and the solution conductivity-based estimation by using Eq. (4).

concentration of the diluted solution was kept constant at 0.01 M. The concentration of the concentrated solution changed with concentration ratios of 5, 10, 50, 100, 150, and 200. The measured membrane potentials of CMV are greater than those of AMV for most cases caused by the higher constant charge density of CMV [44–46]. Calculated by Eq. (14), the permselectivity of the CMV drops from 0.952 to 0.888. Moreover, the membrane potential of AMV also monotonously decreased from 0.959 to 0.866 with an increase in concentration ratio. This tendency can be explained by two reasons. First, the concentration difference induces osmotic dwelling, which is when strong osmotic cling occurs because of high osmotic pressure between the membrane's internal solution and the bulk solution [22, 41, 47, 48]. Next, the possibility of co-ions percolation rises to a higher degree with a higher concentration ratio gradient due to an increase of the CP phenomena, and this leads to an increase at a higher concentration difference ratio [30, 41, 43]. A new data set of the permselectivity is acquired when the operating temperature varies. For the electrical conductivity, a similar way should be followed. Because the mechanism of an interaction between ions and membranes is too complexed, the effects of the temperature on the permselectivity is partly studied based on the temperature dependence of the diffusivity of each ion [49, 50].

We calculated the open circuit voltage (OCV) obtained at zero current by applying the actual permselectivity of the IEMs obtained from **Figure 5**. We compared it with the experimental data. A comparison of the OCVs between the calculation and the experiment is displayed in **Figure 6**. The red and black bars represent the simulated and measured values of the OCV, respectively. The flow rate was fixed at 10 mL/min for each cell. The tendency of the simulation results shows in good agreement with the tendency of the experimental results, although the simulation values are slightly higher in all cases. This is due to two main reasons: (1) the uniform flow distribution for the experimental case was not the same completely because of the flow stream variation due to the effect of flow inlet and outlet branches, leading to the

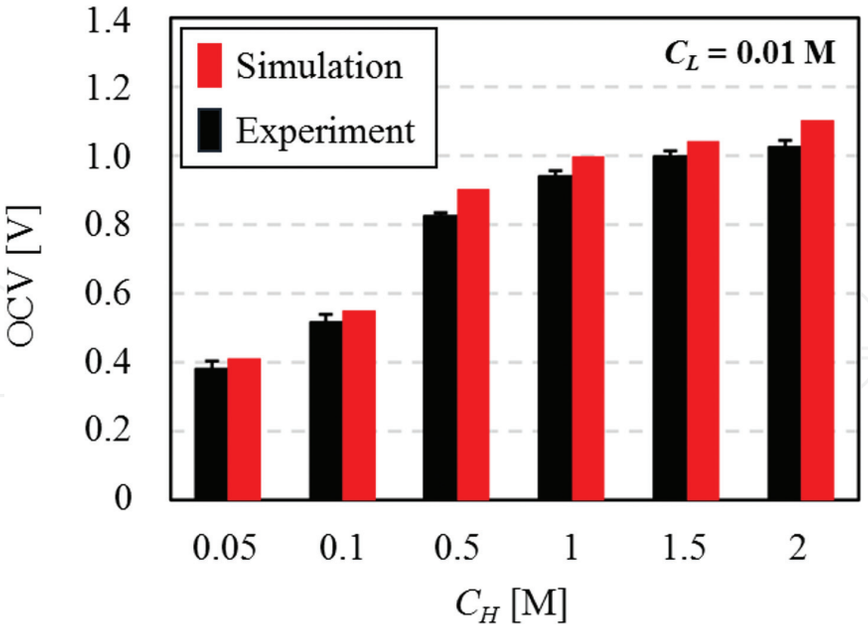

Figure 6. Comparison of the OCV obtained from the simulation and experiment.

production of additional shadow areas [32]. (2) The gaseous bubble (CO_2, NH_3) which is promoted under the room temperature degraded the system performance, while it was not considered in this study [17, 51].

Figure 7 shows the effect of actual permselectivity on RED performance when the concentrated and diluted solutions were fixed as 1 and 0.01 mol, respectively. **Figure 7(a)** and **(b)** show the polarization curves when applying actual permselectivity, and **Figure 7(c)** and **(d)** present the power density curves, calculated with $\alpha = 1$ and the experimentally obtained value $\alpha = 0.891$, respectively. The experimental result is the average of the actual permselectivity of CEM and AEM. The maximum difference of the power density between the calculated and experimental results was 0.2 W/m^2. When we considered the actual permselectivity (in the experiments), however, the gap was reduced to 0.04 W/m^2 (0.5%). Therefore, the consideration of the actual permselectivity plays a critical role in modeling the RED process with ammonium bicarbonate.

4.2. Model validation with experiments

We numerically and experimentally evaluated the power density based on the variation of concentration ratio. The evaluation results are shown in **Figure 8**. In the six cases evaluated, the concentrated solution varied, while the diluted solution was fixed as constant at 0.01 M. The intermembrane distance was 0.3 mm, and the feed flow rate was fixed as 10 mL/min for each cell. The dashed lines represent the simulation results, and the symbols represent the experimental results. When the concentrated solution was equal to or exceeded 1 M, then all the simulation results of the power density curve fall in the error bar area. However, the simulation results deviated from the error bars when the concentrated solution was 0.5 M or less. This phenomenon could be caused by the lower concentration of the concentrated solution which induces an increase of the membrane resistance [24, 52].

http://dx.doi.org/10.5772/intechopen.81006

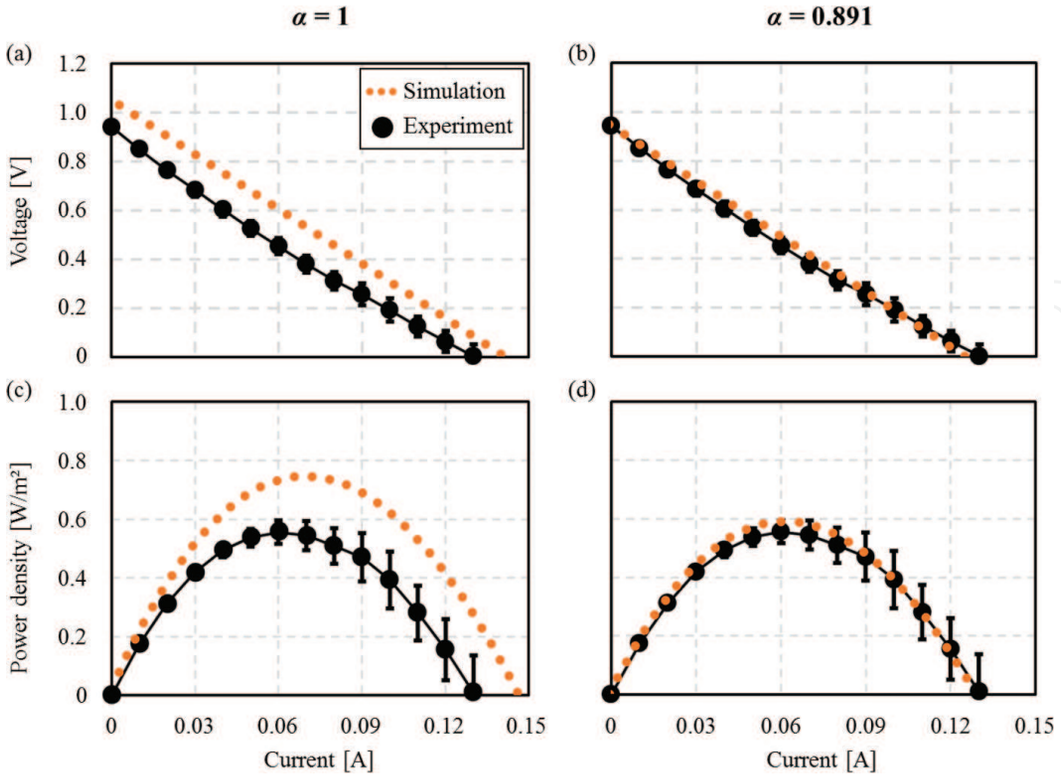

Figure 7. Polarization curves (a) and (b) and power density curves (c) and (d), with actual and ideal permselectivity of the IEM.

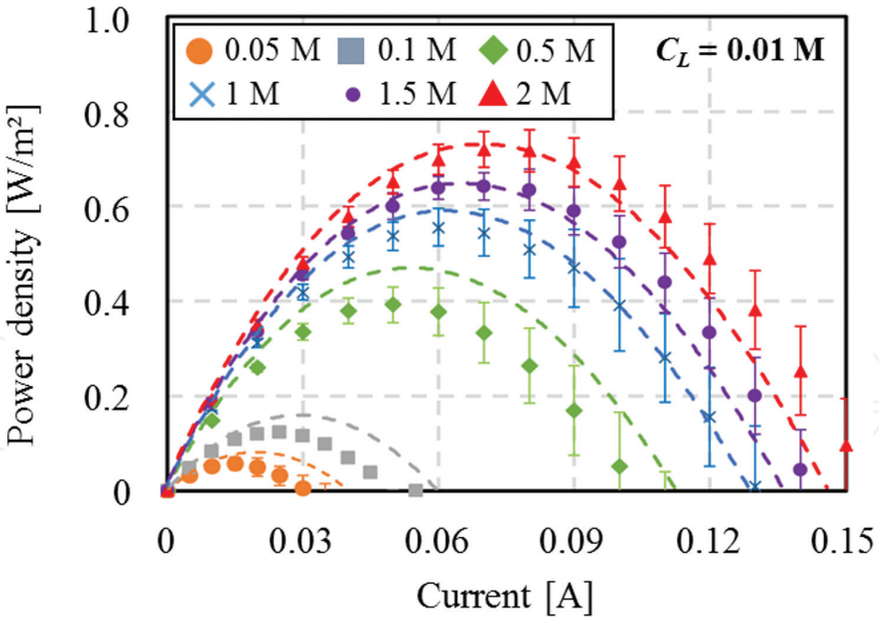

Figure 8. Power density curves with varying concentration ratios. The dashed lines denote the simulation results, and the symbols denote the experimental results.

The change time of the solution in the flow channel depends on the solution feed flow rate. This results in the change of OCV difference between the concentrated and diluted solutions. The influence of the flow rate on the RED system power density and the OCV were estimated.

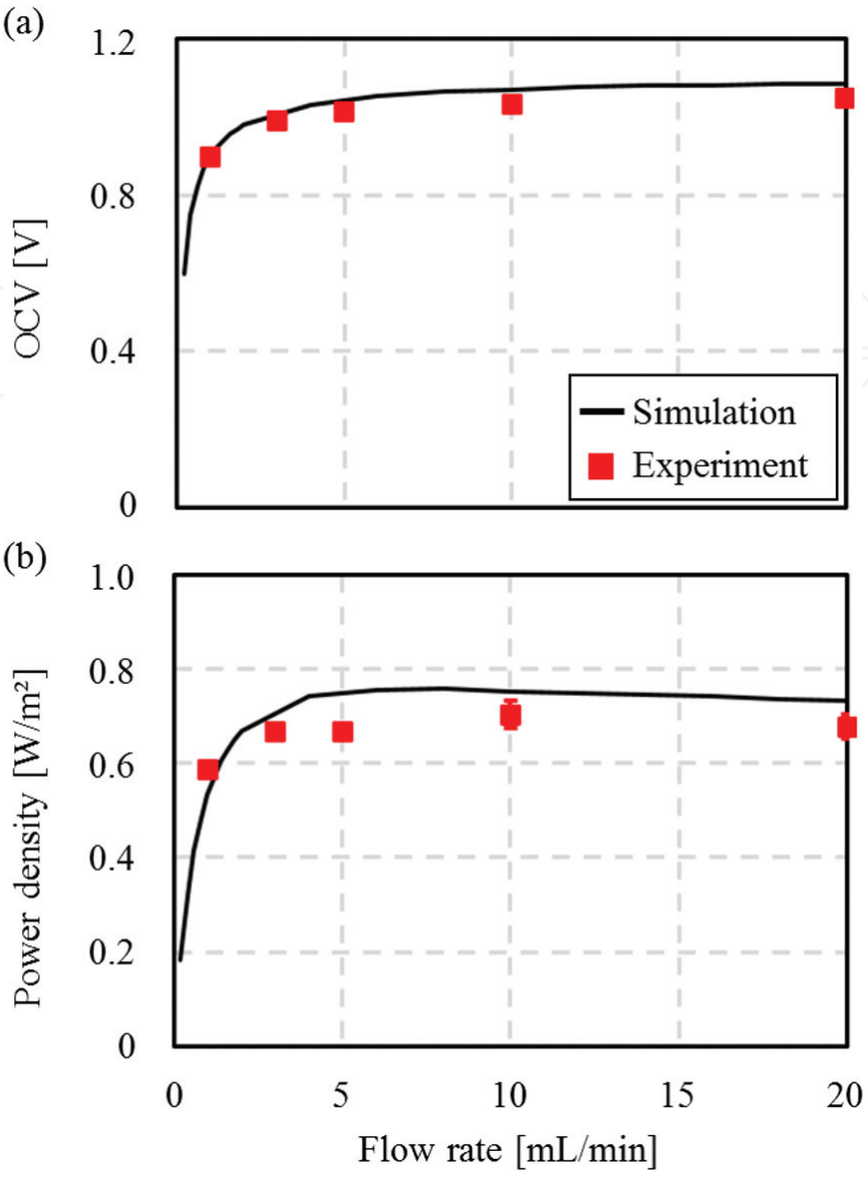

Figure 9. (a) OCV and (b) power density with varying flow rates.

The power density is given in **Figure 9(a)** where the OCV was varied with the solution flow rate simulated from 0.1 mL to 20 mL/min. The diluted and concentrated solutions were kept constant at 2 and 0.01 M, respectively. The intermembrane distance was configured at 0.3 mm. The OCV was increased rapidly below 2 mL/min. Then, it was almost saturated when the flow rate was over 5 mL/min. It shows that the calculated results quite match with the experimental ones.

Figure 9(b) shows the effect of flow rate on power density of the system. The simulation results of power density also showed a slightly different trend from that of OCV. It firstly showed a steep increase below 2 mL/min and then showed a maximum value at a flow rate value of 8 mL/min. After the power density reached a maximum value, it decreased gradually. Overall, the simulation can predict the power density trend very well.

http://dx.doi.org/10.5772/intechopen.81006

4.3. RED system performance prediction and optimization

The flow rate and the intermembrane distance terms in Eqs. (5), (12), and (13) are vital parameters of the RED system. These two parameters influence the residence time in such a way that they control the mixing rate and the internal resistance of the system. In the part, the RED performance in terms of the flow rate and the intermembrane distance was validated by using the aforementioned model. **Figure 10(a)** shows the power density relative to the intermembrane distance. The feed solution flow rate in the channel was set at a constant value of 10 mL/min. Both intermembrane distances for the two compartments were varied from 0.02 to 1 mm. The rich and lean solutions were configured at 2 and 0.01 M, respectively. When the

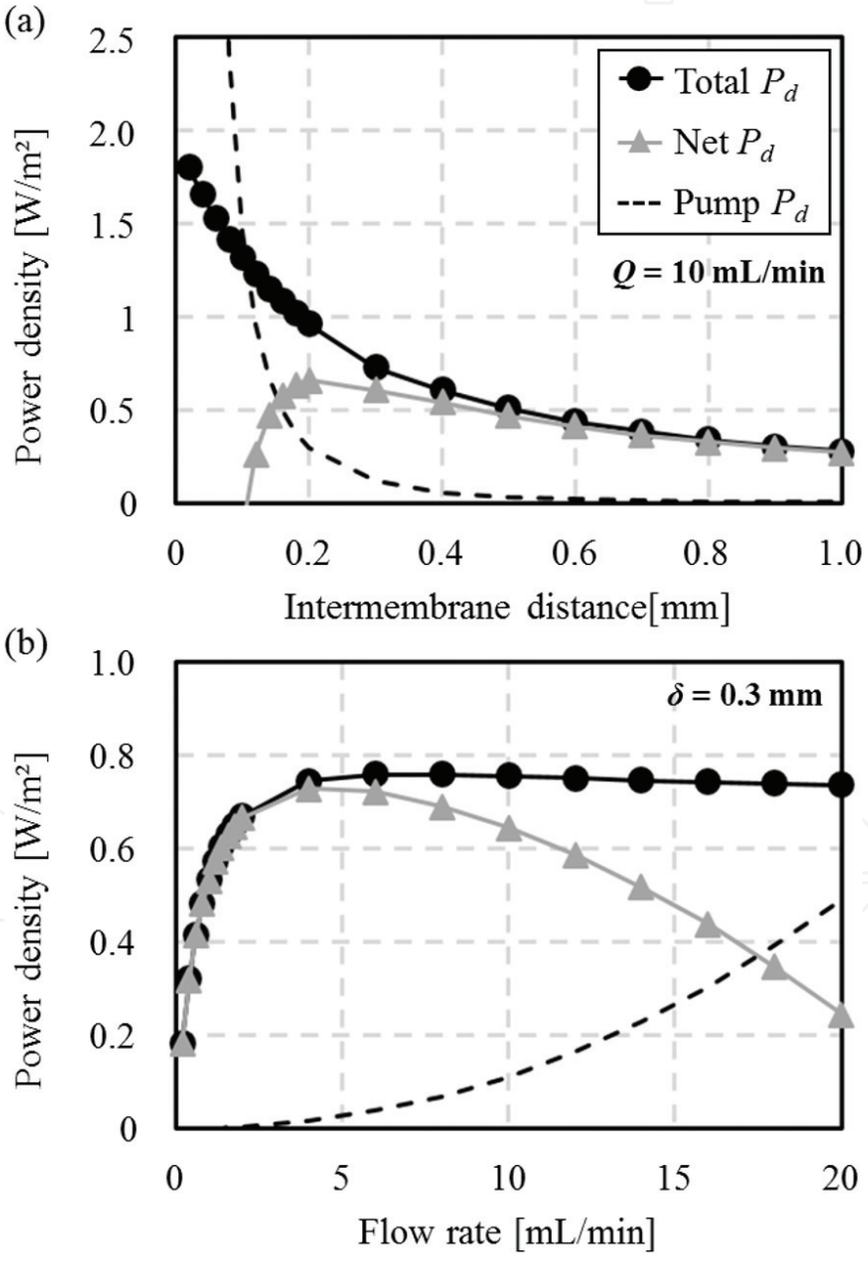

Figure 10. Three different power densities (P_d) of RED relative to (a) intermembrane distance and (b) flow rate.

intermembrane distance was less than 0.5 mm, the power density is increased evidently and arrived at 1.8 W/m^2 at an intermembrane distance of 0.02 mm.

Here, we also considered the pumping loss in the RED system. This can help us to develop the actual RED system in practice [53, 54]. The pumping loss is proportional to the pressure drop, Δp, between the inlet and outlet of the channel, while the flow rate Q is inversely proportional to the pump efficiency, η_{pump}, as listed in Eq. (15):

$$P_{pump}^{RED} = \frac{\Delta p_H Q_H^{RED} + \Delta p_L Q_L^{RED}}{\eta_{pump}} \tag{15}$$

The pumping loss can be normalized to the effective ion exchange area as Eq. (16):

$$P_{pump}^{RED} = \frac{P_{pump}^{RED}}{2LW} \tag{16}$$

The pressure drop was modeled as the well-known Darcy-Weisbach equation, which considers the effect of the spacer [54], as follows:

$$\Delta p = \frac{12\mu L^2}{0.25 d_h^2 t} \tag{17}$$

$$d_h = \frac{4n}{\left(\frac{2}{\delta}\right) + (1-n)\left(\frac{8}{\delta}\right)} \tag{18}$$

Here, μ denotes the viscosity (25°C), and d_h denotes the hydraulic diameter considering the effect of the spacer porosity n.

Figure 10(a) shows the effect of intermembrane distance on power density including the pumping loss. The pumping loss increases greatly when the intermembrane distance is smaller than 0.3 mm. We calculated the power density by subtracting the pumping loss from the total power. The net power density reached a maximum value at the intermembrane distance of 0.2 mm, and then, it was reduced to below zero at 0.1 mm. This is due to the high pumping loss. **Figure 10(b)** shows the relation between the power density and the flow rate when the intermembrane distance was specified at 0.3 mm, and the rich and lean solutions were 2 and 0.01 M, respectively. The highest power density value was 0.76 W/m^2 at a flow rate of 6 mL/min. The optimal value of 0.73 W/m^2 for the net power density was obtained at a flow rate of 4 mL/min. Afterwards, the power density decreased gradually.

Figure 11 shows the effects of the intermembrane distance (δ), the flow rate (Q), and the concentration ratio on the net power density. In this figure, the net power densities arrived their maximum values of 0.85 W/m^2 at δ = 0.1 mm and Q = 3 mL/min, 0.82 W/m^2 at δ = 0.2 mm and Q = 4 mL/min, and 0.73 W/m^2 at δ = 0.3 mm and Q = 5 mL/min.

The highest net power density is obtained when δ = 0.1 mm. The flow rate has a very important impact on the system performance due to the high pumping loss. However, it is less sensitive

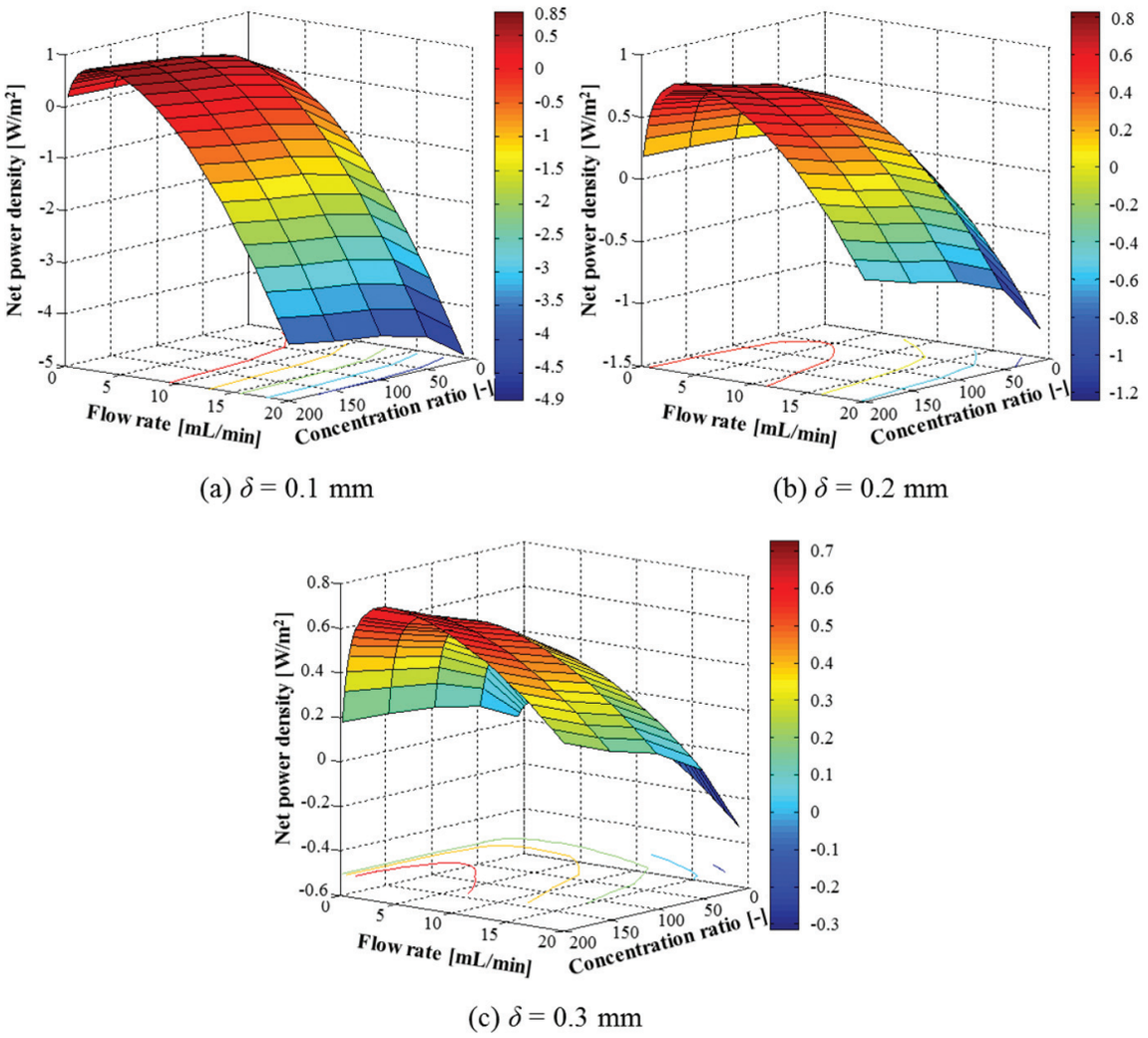

Figure 11. Optimization of net power density with changes in flow rate and concentration ratio. The intermembrane distances (δ) are (a) 0.1, (b) 0.2, and (c) 0.3 mm, and the diluted solution was fixed at 0.01 M.

to the concentration ratio. For the case of δ = 0.3 mm, the performance was less sensitive to the flow rate, whereas it was more sensitive to the concentration ratio.

5. Conclusion

An ammonium bicarbonate-based RED system operating as a closed-loop system was designed to convert low-grade waste heat into electricity. It is possible to harness a variety of waste heat such as released from industrial plants and vehicles or generated by geothermal and solar heat. In this chapter, a mathematical model for the power generation from a RED system used NH_4HCO_3 instead of NaCl. The properties of NH_4HCO_3 were used, and the activity of NH_4HCO_3 in the Nernst equation was substituted by the electrical conductivity via the Planck-Henderson equation. The molar conductivity of NH_4HCO_3 was also replaced by a calculated value. To predict the performance of the RED system, it is very important to measure the membrane potential precisely so as to obtain the actual permselectivity.

The model simulation showed an accurate estimation of the OCV within a wide range of flow rates and concentration ratios. The simulation results also fit well for power density with the experimental results relative to the various flow rates and concentration ratios. Especially, when the concentrated solution is equal to or exceeds 1 M, which is a preferable operating condition for high power generation. The difference between the simulation and experiment for the solution with lower concentration could be potentially attributed to the concentration of electrolytes, which affects the membrane resistance. The improvement in the membrane resistance model with the concentration variation is an interesting topic in order to obtain a better estimation.

We evaluated the net power density through the validated model including the pumping loss as a function of the flow rate, intermembrane distance, and concentration ratio. Consequently, the best performance for the working parameters was obtained. When we fixed the intermembrane distance at 0.1 mm and the flow rate was 3 mL/min, we obtained the highest net power density of 0.84 W/m^2 with the feed solution concentration ratio was 200 (2 M/0.01 M).

The results of this study can help to improve our understanding of the RED system with ammonium bicarbonate. This study also provides a good reference for the RED system modeling to get a higher energy density by using NH_4HCO_3 or other compounds.

Acknowledgements

The study was supported by a National Research Foundation of Korea (NRF) grant funded by the Korean government (MEST) (No. NRF-2014R1A2A2A01003618).

Nomenclature

C	solution concentration [M]
D	diffusion coefficient [m^2/s]
F	Faraday constant [96485 C/mol]
I	electric current [A]
J	molar flux [mol/m^{2}s]
L	length [m]
P	power [W]
Q	volumetric flow rate [mL/min]
R	resistance [Ω]
R_g	universal gas constant [8.314 J/mol·K]
T	ambient temperature [K]

V	electric voltage [V]
V_w	molar volume of water [mol/m^3]
W	width [m]
d_h	hydraulic diameter [m]
h	membrane thickness [m]
t_i	transport number of ion species i [-]
i	current density [A/m^2]
n	porosity [-]
p	power density [W/m^2]
t	residence time [s]
z_i	valence number of ion species i [-]

Greek symbols

Δp	pressure drop [Pa]
Λ	molar conductivity [S·m^2/mol]
α	permselectivity [-]
β	open ratio [-]
γ	activity coefficient [-]
δ	intermembrane distance [m]
ε	permittivity [F/m]
η_{pump}	pump efficiency [-]
μ	viscosity [Pa·s]

Subscripts

H	high concentration solution
L	low concentration solution
CEM	cation exchange membrane
AEM	anion exchange membrane

Acronyms

RED	reverse electrodialysis
$_4$Ha	Ammonium bicarbonate
ORC	organic Rankine cycle

SGE	salinity gradient energy
IEM	ion exchange membrane
CP	concentration polarization
TDEG	thermal-driven electrochemical generator
PMMA	polymethyl methacrylate
CEM	cation exchange membrane
AEM	anion exchange membrane
OCV	open circuit voltage

Author details

Deok Han Kim, Byung Ho Park, Kilsung Kwon, Longnan Li and Daejoong Kim*

*Address all correspondence to: daejoong@sogang.ac.kr

Department of Mechanical Engineering, Sogang University, Seoul, Republic of Korea

References

[1] Oluleye G, Jobson M, Smith R, Perry SJ. Evaluating the potential of process sites for waste heat recovery. Applied Energy. 2016;**161**:627-646

[2] Lu H, Price L, Zhang Q. Capturing the invisible resource: Analysis of waste heat potential in Chinese industry. Applied Energy. 2016;**161**:497-511

[3] Hung TC, Shai TY, Wang SK. A review of organic Rankine cycles (ORCs) for the recovery of low-grade waste heat. Energy. 1997;**22**:661-667

[4] Chen H, Goswami DY, Stefanakos EK. A review of thermodynamic cycles and working fluids for the conversion of low-grade heat. Renewable and Sustainable Energy Reviews. 2010;**14**:3059-3067

[5] Elsheikh MH, Shnawah DA, Sabri MFM, Said SBM, Hassan MH, Bashir MBA, et al. A review on thermoelectric renewable energy: Principle parameters that affect their performance. Renewable and Sustainable Energy Reviews. 2014;**30**:337-355

[6] Tritt TM. Thermoelectric phenomena, materials, and applications. Annual Review of Materials Research. 2011;**41**:433-448

[7] Alam H, Ramakrishna S. A review on the enhancement of figure of merit from bulk to nano-thermoelectric materials. Nano Energy. 2013;**2**:190-212

[8] Lecompte S, Huisseune H, van den Broek M, De Schampheleire S, De Paepe M. Part load based thermo-economic optimization of the organic Rankine cycle (ORC) applied to a combined heat and power (CHP) system. Applied Energy. 2013;**111**:871-881

[9] Mondejar ME, Ahlgren F, Thern M, Genrup M. Quasi-steady state simulation of an organic Rankine cycle for waste heat recovery in a passenger vessel. Applied Energy. 2016; in the press

[10] Luo X, Cao X, Mo Y, Xiao K, Zhang X, Liang P, et al. Power generation by coupling reverse electrodialysis and ammonium bicarbonate: Implication for recovery of waste heat. Electrochemistry Communications. 2012;**19**:25-28

[11] Mikhaylin S, Bazinet L. Fouling on ion-exchange membranes: Classification, characterization and strategies of prevention and control. Advances in Colloid and Interface Science. 2016;**229**:34-56

[12] Daniilidis A, Herber R, Vermaas DA. Upscale potential and financial feasibility of a reverse electrodialysis power plant. Applied Energy. 2014;**119**:257-265

[13] Logan BE, Elimelech M. Membrane-based processes for sustainable power generation using water. Nature. 2012;**488**:313-319

[14] McGinnis RL, McCutcheon JR, Elimelech M. A novel ammonia–carbon dioxide osmotic heat engine for power generation. Journal of Membrane Science. 2007;**305**:13-19

[15] Nam JY, Cusick RD, Kim Y, Logan BE. Hydrogen generation in microbial reverse-electrodialysis electrolysis cells using a heat-regenerated salt solution. Environmental Science and Technology. 2012;**46**:5240-5246

[16] Cusick RD, Kim Y, Logan BE. Energy capture from thermolytic solutions in microbial reverse-electrodialysis cells. Science. 2012;**335**:1474-1477

[17] McCutcheon JR, McGinnis RL, Elimelech M. Desalination by ammonia–carbon dioxide forward osmosis: Influence of draw and feed solution concentrations on process performance. Journal of Membrane Science. 2006;**278**:114-123

[18] McGinnis RL, Elimelech M. Energy requirements of ammonia-carbon dioxide forward osmosis desalination. Desalination. 2007;**207**:370-382

[19] Bevecqua M, Carubia A, Cipollina A, Tamburini A, Dedesco M, Micale G. Performance of a RED system with ammonium hydrogen carbonate solutions. Desalination and Water Treatment. 2016:1-12

[20] Kwon K, Park BH, Kim D. Parametric study of reverse electrodialysis using ammonium bicarbonate solution for low-grade waste heat recovery. Energy Conversion and Management. 2015;**103**:104-110

[21] Geise GM, Cassady HJ, Paul DR, Logan BE, Hickner MA. Specific ion effects on membrane potential and the permselectivity of ion exchange membranes. Physical Chemistry Chemical Physics. 2014;**16**:21673-21681

[22] Geise GM, Hickner MA, Logan BE. Ionic resistance and permselectivity tradeoffs in anion exchange membranes. ACS Applied Materials and Interfaces. 2013;**5**:10294-10301

[23] Geise GM, Hickner MA, Logan BE. Ammonium bicarbonate transport in anion exchange membranes for salinity gradient energy. ACS Macro Letters. 2013;**2**:814-817

[24] Geise M, Curtis AJ, Hatzell MC, Hickner MA, Logan BE. Salt concentration differences alter membrane resistance in reverse electrodialysis stacks. 2014:36-39

[25] Veerman J, Saakes M, Metz SJ, Harmsen GJ. Reverse electrodialysis: A validated process model for design and optimization. Chemical Engineering Journal. 2011;**166**:256-268

[26] Tedesco M, Cipollina A, Tamburini A, Bogle IDL, Micale G. A simulation tool for analysis and design of reverse electrodialysis using concentrated brines. Chemical Engineering Research and Design. 2014;**93**:441-456

[27] Huang W, Walker WS, Kim Y. Junction potentials in thermolytic reverse electrodialysis. Desalination. 2015;**369**:149-155

[28] Tedesco M, Cipollina A, Tamburini A, van Baak W, Micale G. Modelling the reverse electrodialysis process with seawater and concentrated brines. Desalination and Water Treatment. 2012:1-21

[29] Veerman J, de Jong RM, Saakes M, Metz SJ, Harmsen GJ. Reverse electrodialysis: Comparison of six commercial membrane pairs on the thermodynamic efficiency and power density. Journal of Membrane Science. 2009;**343**:7-15

[30] Baker RW. Membrane Technology and Applications. 2nd ed. John Wiley & Sons Ltd.; 2004. pp. 53-58

[31] Bard AJ, Faulkner LR. Electrochemical Methods Fundamentals and Applications. 2nd ed. John Wiley & Sons Inc; 2001. pp. 44-86

[32] Kwon K, Han J, Park BH, Shin Y, Kim D. Brine recovery using reverse electrodialysis in membrane-based desalination processes. Desalination. 2015;**362**:1-10

[33] Hong JG, Zhang W, Luo J, Chen Y. Modeling of power generation from the mixing of simulated saline and freshwater with a reverse electrodialysis system: The effect of monovalent and multivalent ions. Applied Energy. 2013;**110**:244-251

[34] Weinstein JN, Leitz FB. Electric power from differences in salinity: The dialytic battery. Science. 1976;**191**:557-559

[35] Clampitt BH, Kiviat FE. Energy recovery from saline water by means of electrochemical cells. Source. 2015;**194**:719-720

[36] Jagur-Grodzinski J, Kramer R. Novel process for direct conversion of free energy of mixing into electric power. Industrial and Engineering Chemistry Process Design and Development. 1986;**25**:443-449

[37] Veerman J, Post JW, Saakes M, Metz SJ, Harmsen GJ. Reducing power losses caused by ionic shortcut currents in reverse electrodialysis stacks by a validated model. Journal of Membrane Science. 2008;**310**:418-430

[38] Lacey RE. Energy by reverse electrodialysis. Ocean Engineering. 1980;**7**:1-47

[39] Dlugolecki P, Nymeijer K, Metz S, Wessling M. Current status of ion exchange membranes for power generation from salinity gradients. Journal of Membrane Science. 2008;**319**:214-222

[40] Vila J, Gines P, Pico JM, Franjo C, Jimenez E, Varela LM, et al. Temperature dependence of the electrical conductivity in EMIM-based ionic liquids: Evidence of Vogel–Tamman–Fulcher behavior. Fluid Phase Equilibria. 2006;**242**:141-146

[41] Hosseini SM, Madaeni SS, Khodabakhshi AR. The electrochemical characterization of ion exchange membranes in different electrolytic environments: Investigation of concentration and ph effects. Separation Science and Technology. 2012;**47**:455-462

[42] Xu T, Hu K. A simple determination of counter-ionic permselectivity in an ion exchange membrane from bi-ionic membrane potential measurements: Permselectivity of anionic species in a novel anion exchange membrane. Separation and Purification Technology. 2004;**40**:231-236

[43] Sata T. Ion exchange membrane: Preparation, characterization, modification and application. The Royal Society of Chemistry. 2004:102-104

[44] Hong JG, Zhang B, Glabman S, Uzal N, Dou X, Zhang H, et al. Potential ion exchange membranes and system performance in reverse electrodialysis for power generation: A Review. Journal of Membrane Science. 2015

[45] McCormick P, Pellegrino J, Mantovani F, Sarti G. Water, salt, and ethanol diffusion through membranes for water recovery by forward (direct) osmosis processes. Journal of Membrane Science. 2008;**325**:467-478

[46] Wenzlaff A, Boddeker KW, Hattenbach K. Pervaporation of water-ethanol through ion exchange membranes. Journal of Membrane Science. 1985;**22**:333-344

[47] Długołęcki P, Anet B, Metz SJ, Nijmeijer K, Wessling M. Transport limitations in ion exchange membranes at low salt concentrations. Journal of Membrane Science. 2010;**346**: 163-171

[48] Tuan LX, Buess-Herman C. Study of water content and microheterogeneity of CMS cation exchange membrane. Chemical Physics Letters. 2007;**434**:49-55

[49] Bastug T, Kuyucak S. Temperature dependence of the transport coefficient of ions from molecular dynamics simulations. Chemical Physics Letters. 2005;**408**:84-88

[50] Wood JA, Benneker AM, Lammertink RG. Temperature effects on the electrohydrodynamic and electrokinetic behaviour of ion-selective nanochannels. Journal of Physics: Condensed Matter. 2016;**28**:1-9

[51] Hatzell MC, Logan BE. Evaluation of flow fields on bubble removal and system performance in an ammonium bicarbonate reverse electrodialysis stack. Journal of Membrane Science. 2013;**446**:449-455

[52] Długołecki P, Ogonowski P, Metz SJ, Saakes M, Nijmeijer K, Wessling M. On the resistances of membrane, diffusion boundary layer and double layer in ion exchange membrane transport. Journal of Membrane Science. 2010;**349**:369-379

[53] Pawlowski S, Sistat P, Crespo JG, Velizarov S. Mass transfer in reverse electrodialysis: Flow entrance effects and diffusion boundary layer thickness. Journal of Membrane Science. 2014;**471**:72-83

[54] Vermaas DA, Guler E, Saakes M, Nijmeijer K. Theoretical power density from salinity gradients using reverse electrodialysis. Energy Procedia. 2012;**20**:170-184